BRAIN
ORIGINAL ARTICLE

VEGF signalling causes stalls in brain capillaries and reduces cerebral blood flow in Alzheimer's mice

Muhammad Ali, Kaja Falkenhain, Brendah N. Njiru, Muhammad Murtaza-Ali, Nancy E. Ruiz-Uribe, Mohammad Haft-Javaherian, Stall Catchers, Nozomi Nishimura, Chris B. Schaffer and Oliver Bracko†

Increased incidence of stalled capillary blood flow caused by adhesion of leucocytes to the brain microvascular endothelium leads to a 17% reduction of cerebral blood flow and exacerbates short-term memory loss in multiple mouse models of Alzheimer's disease.

Here, we report that vascular endothelial growth factor (VEGF) signalling at the luminal side of the brain microvasculature plays an integral role in the capillary stalling phenomenon of the APP/PS1 mouse model.

Administration of the anti-mouse VEGF-A164 antibody, an isoform that inhibits blood–brain barrier hyperpermeability, reduced the number of stalled capillaries within an hour of injection, leading to an immediate increase in average capillary blood flow but not capillary diameter. VEGF-A inhibition also reduced the overall endothelial nitric oxide synthase protein concentrations, increased occludin levels and decreased the penetration of circulating Evans Blue dye across the blood–brain barrier into the brain parenchyma, suggesting increased blood–brain barrier integrity. Capillaries prone to neutrophil adhesion after anti-VEGF-A treatment also had lower occludin concentrations than flowing capillaries.

Taken together, our findings demonstrate that VEGF-A signalling in APP/PS1 mice contributes to aberrant endothelial nitric oxide synthase /occludin-associated blood–brain barrier permeability, increases the incidence of capillary stalls, and leads to reductions in cerebral blood flow. Reducing leucocyte adhesion by inhibiting luminal VEGF signalling may provide a novel and well-tolerated strategy for improving brain microvascular blood flow in Alzheimer's disease patients.

Meinig School of Biomedical Engineering, Cornell University, Ithaca, NY 14853, USA

†Present address: Department of Biology, University of Miami, Coral Gables, FL 33146, USA

Correspondence to: Oliver Bracko
Meinig School of Biomedical Engineering, Cornell University, Ithaca, NY, USA
E-mail: ob84@cornell.edu or oliver.bracko@miami.edu

Keywords: Alzheimer's disease; capillary stalling; cerebral blood flow; vascular endothelial growth factor; blood–brain barrier

Abbreviations: 2PEF = two-photon excited fluorescence; BBB = blood–brain barrier; CBF = cerebral blood flow; ELISA = enzyme-linked immunosorbent assay; eNOS = endothelial nitric oxide synthase; RBC = red blood cell; VEGF = vascular endothelial growth factor

Received April 01, 2021. Revised July 09, 2021. Accepted September 22, 2021. Advance access publication January 20, 2022

Introduction

Vascular dysfunction plays a critical role in the pathogenesis of Alzheimer's disease and other forms of dementia. Many conditions that drive altered vascular structure and impaired vascular function, including hypertension, obesity, type 2 diabetes and atherosclerosis, are primary risk factors for Alzheimer's disease and other dementias.[1] In addition, both Alzheimer's disease patients and mouse models of Alzheimer's disease show cerebral blood flow (CBF) reductions of 10–30%, beginning in the early stages of disease pathogenesis and continuing through disease progression.[2–4] Within the Alzheimer's disease population, there is also evidence that more severely impaired CBF is associated with poorer cognitive performance.[5] Even in older humans with no neurodegenerative disorder, lower blood flow in the hippocampus is associated with poorer spatial memory.[6] Despite decades of data establishing clear links between CBF deficits and greater dementia risk and severity, the underlying mechanisms causing CBF deficits in Alzheimer's disease or other dementias are only beginning to be revealed, as are the mechanisms by which vascular risk factors contribute to Alzheimer's disease pathogenesis.

We recently found that leucocyte obstructions in cortical capillary segments occur more frequently in multiple mouse models of Alzheimer's disease as compared to wild-type mice. We further found that administering an antibody against the neutrophil-specific cell surface protein lymphocyte antigen 6 complex (Ly6G) led to a ~60% decrease in the incidence of non-flowing capillaries and a ~20% increase in CBF, all within 10 min. This CBF increase was correlated with improvements in performance on spatial and short-term memory tasks in the Alzheimer's disease mice that were apparent at 3 h after anti-Ly6G administration.[7] This work has suggested that interfering with neutrophils adhering in capillary segments could be a novel therapeutic approach for Alzheimer's disease making efforts to elucidate the molecular signalling that links Alzheimer's disease pathogenesis to increased incidence of capillary stalling critical.

Vascular endothelial growth factor (VEGF-A) is involved in signalling pathways that drive a broad variety of physiological processes including angiogenesis,[8] vascularization,[9] lymphangiogenesis,[10] growth tip guidance,[11] vascular dysfunction,[9] response to fluid shear stress,[12] cellular junction integrity,[9] neurogenesis[11] and neuroprotection.[8] With such a complex set of downstream impacts, it is not surprising that alterations of VEGF-A signalling have been found to have a wide range of effects in the CNS and in the periphery. VEGF-A is secreted into the blood from many tissues and several transport routes such as lymphatic drainage, microvascular permeability, internalization, and plasma clearance. The source and route of VEGF-A transportation is crucial for its function. For example, VEGF-A levels in the blood regulate blood–brain barrier (BBB) integrity.[13–15] In mouse models of diabetic retinopathy, peripherally inhibiting VEGF-A signalling reduced the incidence of retinal capillary obstructions caused by adhered leucocytes.[16] Additionally, peripheral inhibition of vascular endothelial growth factor receptor-2 (VEGF-2R) lead to improved clearance of microsphere-induced cortical capillary obstructions and a reduction in the pruning of such obstructed capillaries.[17,18] These findings suggest that peripheral VEGF-A signalling plays a critical role in microvascular obstructions and that inhibiting VEGF-A signalling may improve microvascular flow in the CNS.

Differing changes in and impacts of VEGF-A signalling have been observed in Alzheimer's disease, depending largely on whether the focus is on VEGF-A signalling in the periphery or in the brain itself. Several reports have shown increased VEGF-A levels in the blood plasma of Alzheimer's disease patients,[19–22] while the opposite has also been found.[23,24] VEGF-A expression could be disease stage dependent; indeed, a study suggests increased levels of plasma VEGF-A in mild cognitive impairment and early-onset Alzheimer's disease but a reduction in patients with late-onset Alzheimer's disease.[25] In the brain vasculature expression of VEGF-A has been found to be both increased[26,27] and decreased,[28] across different studies, in capillaries and blood vessels from Alzheimer's disease patients. Overall, these studies suggest a very complex pattern of VEGF-A expression in the brain and the vasculature that is mis-regulated in Alzheimer's disease. If vascular VEGF-A signalling is, indeed, increased in Alzheimer's disease, it could contribute to the capillary obstructions, as has been found in mouse models of diabetic retinopathy.[16] On the other hand, VEGF-A signalling plays a supportive role for cells within the CNS, and increased VEGF-A signalling in the brain has been shown to have beneficial effects in Alzheimer's disease mouse models. Specifically, VEGF-A-releasing nanoparticles injected into the brain of APP/PS1 mice improved behavioural deficits and reduced neuronal loss.[29] Here, we hypothesized that peripherally inhibiting VEGF-A signalling may reduce the incidence of non-flowing capillaries in the APP/PS1 mouse models of Alzheimer's disease, thereby increasing CBF.

Using *in vivo* two-photon excited fluorescence (2PEF) microscopy, we examined the impact of peripheral VEGF-A inhibition on the incidence of non-flowing capillaries in the brain microvasculature of the APP/PS1 mouse model of Alzheimer's disease. We used an antibody against the murine VEGF-A165 protein (which we refer to as 'anti-VEGF-A' in this article) that is too large to cross the BBB in significant amounts.[30–32] We quantified the incidence of non-flowing capillaries as well as blood flow speeds in flowing capillaries before and after administration of antibodies against VEGF-A. To unearth potential mechanisms by which VEGF-A regulates capillary obstructions and CBF in the CNS, we examined the expression of proteins associated with the BBB and their function in APP/PS1 mice and controls, as well as from human tissue samples from Alzheimer's disease patients.

Materials and methods

Animals

All animal procedures were approved by the Cornell Institutional Animal Care and Use Committee (protocol number 2015–0029) and were conducted under the oversight of the Cornell Center for Animal Resources and Education. We used the APP/PS1 transgenic mouse model of Alzheimer's disease (B6.Cg-Tg (APPswe, PSEN1dE9) 85Dbo/J; MMRRC_034832-JAX, The Jackson Laboratory), with wild-type littermates as controls.

Experimental cohorts

The experiments were conducted in three cohorts. The first cohort of mice (10–14 months) was divided into four experimental groups: Alzheimer's disease mice given the anti-VEGF-A treatment ($n = 5$; three male, two female), Alzheimer's disease mice given a placebo saline injection ($n = 4$; two male, two female), wild-type mice given the anti-VEGF-A treatment ($n = 6$; three male, three female) and wild-type mice given a placebo saline injection ($n = 6$; three male, three female; Fig. 2A). Each anti-VEGF-A injection consisted of 200 µl of 32.5 pM concentration of antibody against mouseVEGF-A164 protein (AF-493, R&D Systems, Inc.) in saline and was administered intraperitoneally. Control injections consisted of 200 µl of saline. Mice first received cranial windows for imaging (see below) and following a 2–3-week recovery period, anti-VEGF-A injections were administered every other day over a 2-week span. Mice were imaged at the 1-week mark, which was after the first three

injections, and again at the 2-week mark, after the last three injections. After the second imaging session, these mice were sacrificed and their brains were removed for enzyme-linked immunosorbent assay (ELISA) and immunofluorescence.

The second cohort of mice (12–15 months) was divided into two experimental groups: Alzheimer's disease mice ($n = 9$; five male, four female) and wild-type mice ($n = 4$; two male, two female; Fig. 5A). After receiving a cranial window and being given 2–3 weeks to recover, these animals also received anti-VEGF-A injections every 2 days for 1 week, with the same dosage and route of administration as above. With this cohort, mice were first imaged at baseline, 1 h after the first injection, and finally at 1 week after a total of three injections. After the final imaging sessions, these animals were sacrificed and their brains were perfused for qualitative Evans Blue leakage analysis (see below).

The third cohort of mice (9–10 months) was divided into four experimental groups: Alzheimer's disease mice given the anti-VEGF-A treatment ($n = 3$; two male, one female), Alzheimer's disease mice given a placebo saline injection ($n = 3$; two male, one female), wild-type mice given the anti-VEGF-A treatment ($n = 3$; two male, one female) and wild-type mice given the placebo saline injection ($n = 3$; two male, one female; Fig. 6A). These animals were sacrificed 1 h after treatment and their brains were perfused for quantitative Evans Blue leakage analysis.

The fourth cohort of mice (10–11 months) was divided into four experimental groups: Alzheimer's disease mice given the anti-VEGF-A treatment ($n = 3$; one male, two female), Alzheimer's disease mice given a placebo saline injection ($n = 3$; two male, one female), wild-type mice given the anti-VEGF-A treatment ($n = 3$; two male, one female), and wild-type mice given the placebo saline injection ($n = 3$; one male, two female). These animals were sacrificed after 2 weeks of treatment and their brains snap-frozen and used for ELISA assays.

Surgical procedure

The animals were initially anaesthetized with 3% isoflurane and maintained on 1.5% isoflurane in oxygen. They were injected subcutaneously with atropine (54925–063-10, Med-Pharmex), dexamethasone (07-808-8194, Phoenix Pharm) and ketoprofen (Zoetis). The atropine was administered at 0.005 mg per 100-g mouse weight and was used to prevent fluid build-up in the lungs. The dexamethasone was administered at 0.025 mg per 100-g mouse weight and was used to reduce surgery-induced inflammation. The ketoprofen was administered at 0.5 mg per 100-g mouse weight and was used to reduce surgery-induced inflammation and to provide post-surgical analgesia.

The top of the head was shaved using clippers (Oster). The exposed area was washed three times, alternating between a 70% ethanol and an iodine solution (AgriLabs). The mice were then placed on a feedback-control heating blanket (40-90-8D DC, FHC) to maintain body temperature at 37°C. The head was fixed on a custom-built stereotactic surgery frame using ear bars and a bite bar. Bupivacaine (0.1 ml of a 0.125% solution in saline; Hospira) was injected subcutaneously in the scalp to provide a local nerve block. The skin was opened and a 6–7-mm diameter craniotomy was performed on the top of the skull, centred on the midline and about halfway between the lambda and bregma points. This was done with a high-speed drill (HP4-917–21, Fordom), using 0.9-mm diameter drill bits at the top of the skull and switching to 0.7-mm and, finally, 0.5-mm diameter bits when nearly through the skull (Fine Science Tools). The circumscribed bone flap was removed, the brain covered with saline, and the opening covered with an 8-mm diameter glass coverslip (11986309, Thermo Scientific), which was glued to the remaining skull using cyanoacrylate adhesive (Loctite) and dental cement (Co-Oral-Ite Dental).

For 2 days after surgery, the animals were treated with dexamethasone at 0.025 mg per 100-g animal weight and ketoprofen at 0.5 mg per 100-g animal weight, daily. The mice were given at least 2 weeks to recover from this surgery. If the clarity of the optical window was deemed too poor for high-quality 2PEF imaging after the 2 weeks, the mice were sacrificed and discontinued from the study (6 out of 34 mice were removed due to poor cranial windows).

In vivo two-photon microscopy

The animals were initially anaesthetized with 3% isoflurane and maintained on 1.5% isoflurane. They were then placed on a custom-built stereotactic surgery frame, injected with atropine as described above and were placed above a feedback-control heating blanket maintaining body temperature at 37°C. For fluorescent labelling of the microvasculature, 70-kDa Texas Red dextran (40 µl of a 2.5% w/v solution in saline, Thermo Fischer Scientific) was retro-orbitally injected before imaging. Some animals were also retro-orbitally injected with a second syringe containing Rhodamine 6G (0.1 ml of a 1-mg ml^{-1} solution in saline, Acros Organics) to distinguish circulating leucocytes and platelets from red blood cells (RBCs) via mitochondrial labelling. Imaging was conducted using 830-nm, 75-fs pulses from a Ti:sapphire laser oscillator (Vision S, Coherent). The laser beam was raster-scanned using galvanometric scan mirrors at one frame per second. Microvasculature was imaged using a 20× water-immersion objective lens for high-resolution imaging (numerical aperture of 1.0, Carl Zeiss; or numerical aperture of 0.95, Olympus), or a 4× objective (numerical aperture of 0.28, Olympus) for broader mapping of the vascular network on the surface of the cortex. The emitted fluorescence was detected using detection optics that were ray traced to efficiently deliver the divergent cone of light emerging from the back aperture of the objective to the ∼5-mm diameter active area of high quantum efficiency GaAsP photomultiplier tubes (H6527, Hamamatsu).

Fluorescence signalling from the Texas Red dye was detected through a 641/75 nm (centre wavelength/bandwidth) filter and the fluorescence from Rhodamine 6G was detected through a 550/49 nm filter, with the light separated by a long-pass dichroic with a cut-off wavelength of 605 nm. ScanImage software was used to control the laser scanning and data acquisition.[33] Three-dimensional images of the brain microvasculature (Fig. 1A) and line scan measurements of RBC speed in capillaries (Fig. 2C) were acquired using this system. Stacks of images were spaced 1 µm axially and were taken to a depth of 200–400 µm. From within this imaging volume, 6–10 capillary segments, all with a diameter of less than 10 µm, were randomly selected for line scan-based measurement of flow speed and for small image stacks to quantify vessel diameter.

Analysis of capillary speed and diameter

We identified capillary segments that were largely parallel to the cortical surface. We took a small image stack that was later used to determine the diameter of the vessel using the plot profile option on ImageJ. Speeds of RBC flow in these capillaries were determined by repeatedly scanning a line along the central axis of the vessel. Unlabelled RBCs showed up as dark patches inside the vessel lumen, and the movement of these unlabelled RBCs was tracked over successive line scans by constructing a space–time plot, where the x-axis represented distance along the vessel axis and the y-axis represented time. Diagonal stripes on this plot were formed by the moving RBCs and had a slope that was inversely

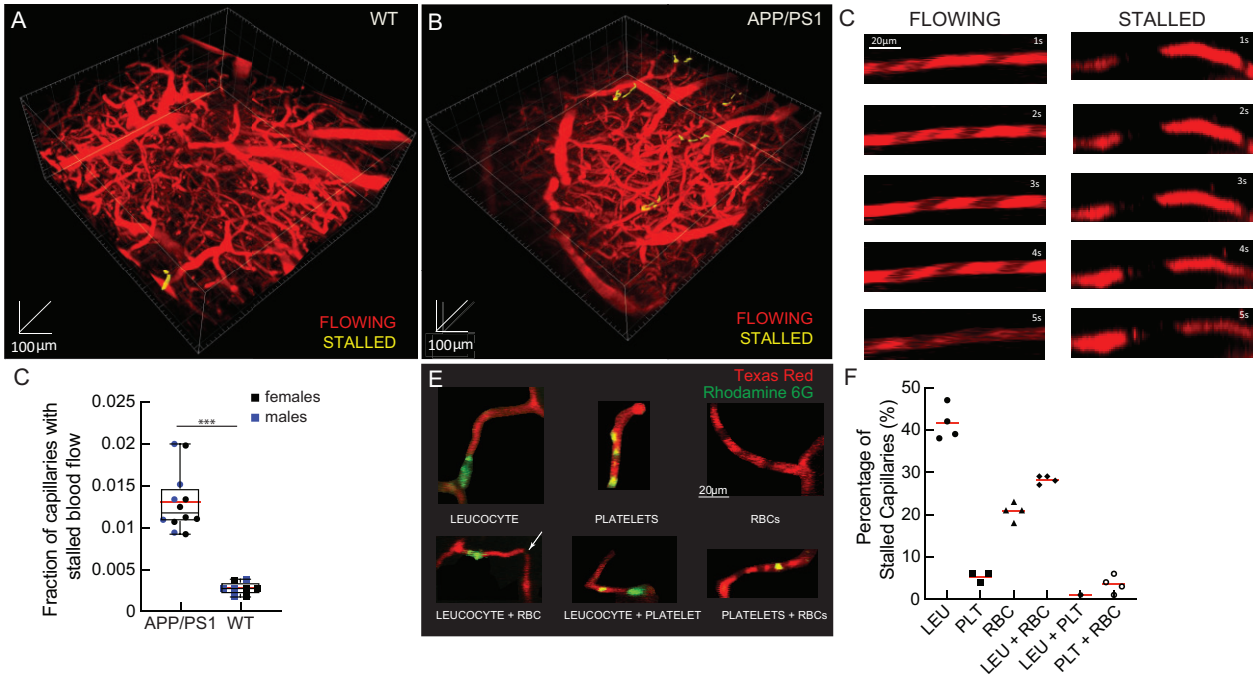

Figure 1 2PEF imaging of mouse cortical vasculature showed a larger fraction of capillaries with stalled blood flow in APP/PS1 mice. Rendering of a 2PEF image stack of the cortical vasculature (red; Texas Red dextran) from a wild-type (WT) mouse (**A**), with a single stalled capillary indicated in yellow, and of an APP/PS1 mouse (**B**), with five stalled capillaries. (**C**) Individual capillaries throughout the image stack were characterized as flowing or stalled based on the movement of unlabeled (black) red blood cells within the fluorescently labelled blood plasma (red). (**D**) Fraction of capillaries with stalled blood flow APP/PS1 ($n = 12$) and WT ($n = 8$) mice, ~ 23 000 capillaries; two-tailed Mann–Whitney test, $P = 0.001$; box plot: whiskers extend 1.5× the difference between the 25th and 75th percentiles of the data, the red horizontal line represents the median, the black line represents the mean. Sex differences are indicated by colour, with black data-points representing females and blue representing males. (**E**) Z-projection of image stacks through stalled capillaries that contain a leucocyte (LEU, *top left*), platelet aggregates (PLT, *top middle*), RBCs (*top right*), LEU and RBCs (*bottom left*), LEU and PLT (*bottom middle*) and PLT and RBCs (*bottom right*), distinguished by fluorescent labels (red: Texas Red labelled blood plasma; green: Rhodamine 6G labelled LEU and PLT). (**F**) Percentage of capillary stalls in APP/PS1 mice that contained only LEU, only PLT, only RBCs, both LEU and RBCs, both LEU and PLT and both PLT and RBCs ($n = 4$, 98 capillaries).

proportional to the RBC speed, which was calculated using a radon transform-based algorithm that has been previously described by.[34]

Crowd-sourced quantification and analysis of capillary stalling

To determine the incidence of non-flowing capillaries within the microvasculature we used a purpose-built citizen science data analysis platform, StallCatchers. We previously detailed and validated this methodology.[35] Briefly, we used the convolutional neural network DeepVess to segment 2PEF stacks into voxels defined to be within or outside of the vasculature.[36] Vessel centrelines were then determined from this segmented image using standard dilation and thinning operations[37] and individual vessel segments were identified. Vessels with diameters greater than 10 µm were excluded in order to restrict our analysis of stalling behaviours to capillaries. Identified capillary segments were outlined and a cropped image stack centred on each outlined capillary was uploaded to www.StallCatchers.com. Volunteers scored each of the ~60 000 capillaries examined in this study as either flowing (0) or stalled (1). Because the Texas Red dextran labels the blood plasma, blood cells were seen as dark patches in the microvasculature lumen. StallCatchers users would determine whether they saw these dark patches move along the vessel axis across the multiple frames in which the outlined capillary was present (minimum of ~5). Multiple volunteers scored each capillary as flowing or stalled. Each volunteer had a unique sensitivity score determined by their performance on intermixed capillaries that had already been scored as stalled or flowing by laboratory members. A weighted 'crowd-confidence' score that took each volunteer's sensitivity into account, ranging from 0 (likely flowing) to 1 (likely stalled), was then determined for each capillary. Capillaries with scores above 0.5 ($n = 900$) were validated by laboraotry members who were blinded to the genotype and treatment status. Capillaries with crowd confidence scores of 0.9–1 were found to be stalled 95% of the time by laboratory members, whereas in those with confidence scores between 0.5 and 0.6, only 1.5% of the capillaries were determined to be stalled by laboratory members. This citizen science scoring of capillary flow reduced the number of capillaries directly examined by laboratory members by a factor of 50. Finally, stall rates were calculated as the number of stalled capillaries divided by the number of total capillaries across all 2PEF images taken for each mouse at each time point. All imaging stacks were manually checked for wrong connection after segmentation.

Upon identifying capillary stalls, in certain animals the Rhodamine 6G channel was used to determine the fraction of stalled capillaries that contained only leucocytes, only platelets, only RBCs, both leucocytes and RBCs, or both platelets and RBCs, using the distinguishing criteria previously described by.[38] All image analysis was conducted using ImageJ software (NIH).

Analysis of vascular density

We calculated the averaged density of the capillary network using the DeepVess[36] for vascular segmentation. We reported the capillary density as the fraction of image voxels determined to be inside vessels divided by the total number of image voxels. Image stacks

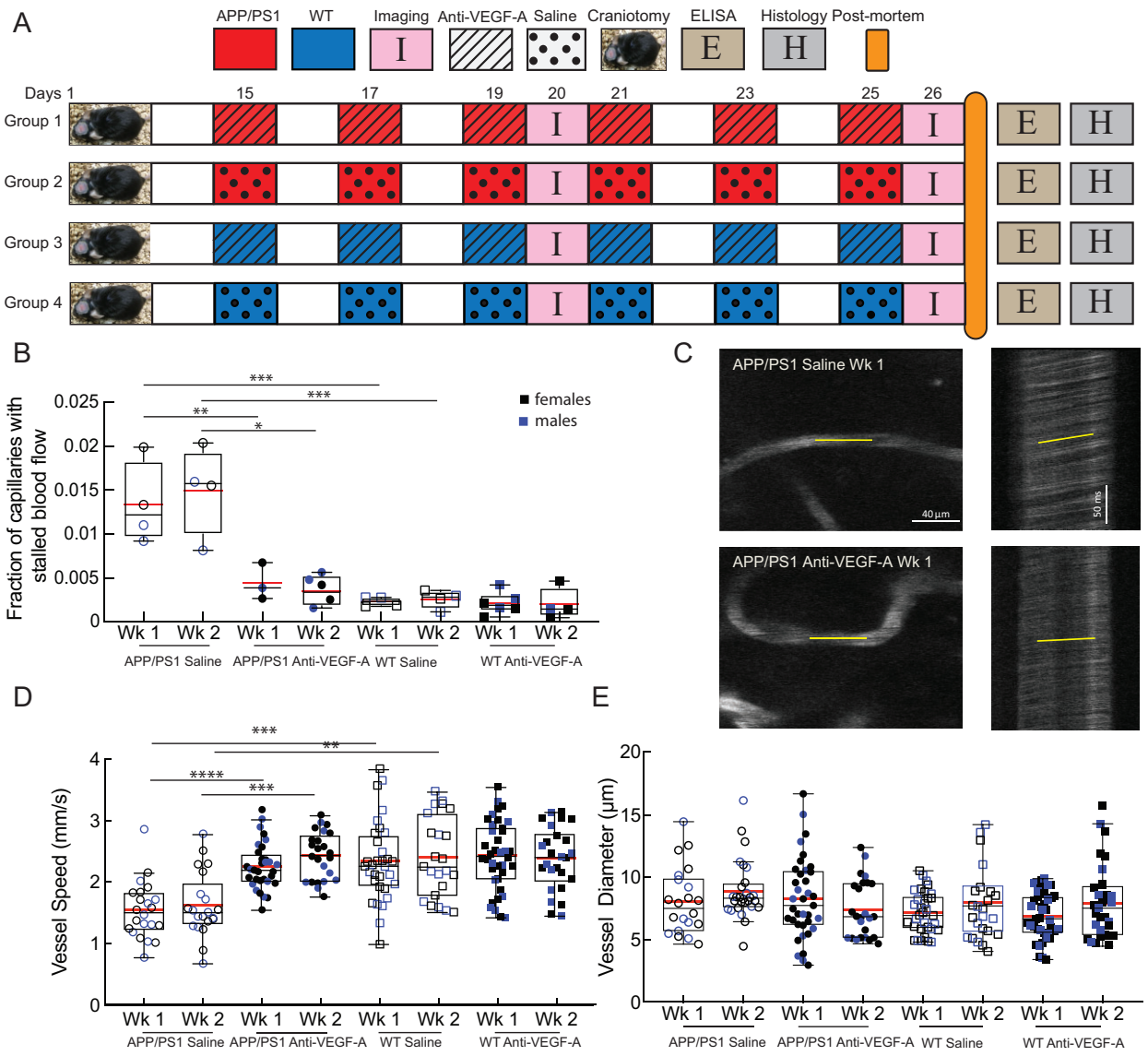

Figure 2 Anti-VEGF-A antibody treatment reduced the incidence of capillary stalling increased CBF speed in APP/PS1 mice. (**A**) Schematic of experimental timeline. After craniotomies were performed and the mice recovered for 2 weeks, the mice were divided into four groups and treated, as follows, every other day for 2 weeks: APP/PS1 mice injected with saline ($n = 4$; APP/PS1–saline), APP/PS1 mice treated with anti-VEGF-A ($n = 5$; APP/PS1–anti-VEGF-A), wild-type (WT) mice injected with saline ($n = 6$; WT–saline) and WT mice treated with anti-VEGF-A ($n = 6$; WT–anti-VEGF-A). These mice were imaged twice, on the sixth and 12th days after the first injection. Their brains were harvested for post-mortem assays after the second imaging session. (**B**) Box plot of the fraction of capillaries with stalled blood flow after 1 week and 2 weeks of anti-VEGF-A or saline treatment in APP/PS1 and WT mice (APP/PS1–anti-VEGF-A: two mice excluded at Week 1 time point due to motion artefact, one mouse lost cranial window before Week 2 time point; WT–saline: one mouse at Week 1 excluded due to motion artefact, one mouse lost cranial window before Week 2; WT–anti-VEGF-A: one mouse lost cranial window before Week 2 imaging session); ~48 000 capillaries; one-way ANOVA with Holm–Šídák *post hoc* multiple comparison correction to compare across multiple groups: Week 1 APP/PS1–saline versus Week 1 APP/PS1–anti-VEGF-A $P = 0.004$, Week 2 saline versus Week 2 anti-VEGF-A APP/PS1 $P = 0.001$, Week 1 saline APP/PS1 versus Week 1 saline WT $P = 0.001$, Week 2 APP/PS1–saline versus Week 2 WT–saline $P = 0.001$, Week 1 APP/PS1–anti-VEGF-A versus Week 1 APP/PS1–saline $P = 0.01$; each data-point in the graph represents the fraction of stalled capillaries in 4–6 2PEF stacks for each mouse). (**C**) Images (*left*) and line scans (*right*) from representative vessels from a saline (*top*) and anti-VEGF-A (*bottom*) injected APP/PS1 mouse. (**D**) RBC flow speed and (**E**) vessel diameter in cortical capillaries after 1 week and 2 weeks of anti-VEGF-A or saline treatment in APP/PS1 and WT mice [Week 1 APP/PS1–saline: $n = 4$, 22 vessels, Week 2 APP/PS1–saline: $n = 4$, 21 vessels, Week 1 APP/PS1–anti-VEGF-A: $n = 5$, 32 vessels, Week 2 APP/PS1–anti-VEGF-A: $n = 4$, 24 vessels (one mouse lost cranial window after Week 1 imaging session), Week 1 WT–saline: $n = 6$, 32 vessels, Week 2 WT–saline: $n = 5$, 23 vessels (one mouse lost cranial window after Week 1 imaging session), Week 1 WT–anti-VEGF-A: $n = 6$, 38 vessels, Week 2 WT–anti-VEGF-A: $n = 5$, 26 vessels (one mouse lost cranial window after Week 1 imaging session)]; one-way ANOVA with Tukey's *post hoc* multiple comparison correction to compare vessel speed across groups: Week 1 saline APP/PS1 versus Week 1 anti-VEGF-A APP/PS1 $P < 0.0001$, Week 2 saline versus Week 2 APP/PS1–anti-VEGF-A $P = 0.0010$, Week 1 WT–saline versus Week 1 WT–anti-VEGF-A $P > 0.99$, Week 2 saline WT versus Week 2 WT–anti-VEGF-A $P > 0.99$, Week 1 APP/PS1–saline versus Week 1 WT–saline $P = 0.0007$, Week 2 APP/PS1–saline versus Week 2 WT–saline $P = 0.0022$, Week 1 APP/PS1–anti-VEGF-A versus Week 1 WT–saline $P > 0.99$, Week 2 APP/PS–anti-VEGF-A 1 versus Week 2 WT–saline $P > 0.99$; each point in the graph represents one of the 4–8 capillaries measured in each mouse at each imaging session. In all graphs the box plot whiskers extend 1.5 × the difference between the 25th and 75th percentiles of the data, the red horizontal line represents the median and the black line represents the mean. Sex differences are indicated by colour, with black data-points representing females and blue representing males.

were first manually masked to exclude large surface vessels from this analysis.

ELISA assay

After 2 weeks of treatment, the mice from the first cohort were sacrificed by a retro-orbital injection of pentobarbital at 5 mg per 100 g mouse weight. Brains were extracted and cut along the centreline. One half was preserved in 4% paraformaldehyde (PFA) in 1× phosphate-buffered saline (PBS) for 24 h and then stored in 30% sucrose solution for histology.[39]

The other half was weighed and homogenized using a Dounce homogenizer (8343–15, ACE GLASS, Inc.) in 1 ml PBS with complete protease inhibitor (Roche Applied Science) and 1 mM of the serine protease inhibitor 4-(2-aminoethyl) benzenesulfonyl fluoride hydrochloride (ThermoFisher Scientific). The samples were sonicated and centrifuged at 14 000*g* for 30 min at 4°C. The PBS-soluble supernatant was separated and stored at –80°C. The remaining pellet was dissolved in 0.5 ml 70% formic acid before being sonicated and centrifuged at 14 000*g* for 30 min at 4°C. The supernatant was separated and neutralized in 1M Tris buffer at a pH of 9.0. Protein concentration was measured using the Pierce BCA Protein Assay (ThermoFisher Scientific). The brain extracts were diluted to equal protein concentration and were analysed by sandwich ELISA for VEGF-A, endothelial nitric oxide synthase (eNOS), amyloid-β_{40}, amyloid-β_{42}, and amyloid-β aggregates using commercial ELISA kits and following the manufacturer's protocols (VEGF-A: ab209882, Abcam; eNOS: ab230938, Abcam; Aβ40: KHB3481, and Aβ42: KHB3441, ThermoFisher Scientific).

Tissue from brain lysates and plasma samples was collected as previously described.[39] Brains were weighed and homogenized using a Dounce homogenizer (8343–15, ACE GLASS, Inc.) in 2 ml PBS with complete protease inhibitor (Roche Applied Science), PhosSTOP (Roche Applied Science) and 1 mM of the serine protease inhibitor 4-(2-aminoethyl) benzenesulfonyl fluoride hydrochloride (ThermoFisher Scientific). The samples were further ruptured using a syringe and centrifuged at 14 000*g* for 30 min at 4°C. The PBS-soluble supernatant was separated and stored at –80°C. After measuring the concentrations, ELISAs were performed following the manufacture's protocol [VEGF1R (MVR100) and VEGF2R (MVR200B): R&D Systems; VEGF-A (ab209882) and eNOS: (ab230938), Abcam]. Peripheral blood drawn using cardiac puncture and centrifuged for 10 min at 3000 rpm (1500*g*) and the plasma was transferred to a new tube. The albumin was removed using the Pierce™ Albumin Depletion Kit (ThermoFisher Scientific). After the measuring the concentrations, ELISAs were performed following the manufacturer's protocol [sVEGF1R (MBS4503308) and sVEGF2R (MBS776967), MyBiosource]. Data were collected through a Synergy HT plate reader (BioTek) and analysed via Gen5 software (BioTek).

Immunohistochemistry and confocal microscopy

The 2-week-treated half-brains preserved for immunofluorescence were placed in optimal cutting temperature compound (Fisher Scientific) and sliced into 30-μm sections. The sections were mounted and washed in PBS. They were incubated in blocking solution, 250 μl of donkey serum and 5 μl of 100% Triton in 5 ml of PBS, for 1 h and then overnight at 4°C in a 1:100 primary antibody solution of the anti-GLUT-1 capillary marker antibody (ab15309, Abcam) and the BBB integrity protein occludin anti-Occludin antibody (ab31721, Abcam) in blocking solution. The following day, the samples were washed in PBS and incubated for 1.5 h in a 1:300 secondary antibody solution of a 488 nm anti-mouse antibody (ThermoFisher Scientific) and a 594 nm anti-rabbit antibody (ThermoFisher Scientific). The sections were washed three times in PBS and allowed to thoroughly dry and coverslips were added onto the slides.

The slides were imaged using confocal microscopy on three-channels. Z-stacks were taken from the pre-frontal cortex, somatosensory cortex, parietal lobe and hippocampus up to 30 μm deep. The same gain and excitation limits were used across all samples. For broad analysis of the vasculature, each stack of images was converted to a single Z project. The Renyi entropy filter on ImageJ was applied, and individual particles were outlined. Integrated density was calculated for each channel (Supplementary Fig. 1). Results were reported as 'integrated density of occludin/integrated density of GLUT-1'. Analysis of specific vessels entailed outlining entire capillaries, from one end to the other. ImageJ's mean grey value function was applied to this outline, specifically on the occludin channel. These results were reported as 'mean occludin intensity throughout capillary length'.

Human staining

Post-mortem human cortical tissue from males and females were obtained through the NIH NeuroBioBank. Frozen cortical brain samples were fixed in formalin or were received in formalin from the brain bank. Sections 30-μm thick were sectioned in a cryostat and stored in cryoprotection solution until further processing. Cortical brain sections were rinsed for 5 min with 1× PBS and incubated with a 0.3% solution of Sudan Black B in 70% ethanol for 30 min to reduce lipofuscin autofluorescence. Slices were then blocked in 3% goat serum for 30 min and incubated with primary antibody overnight at 4°C. The next day, slices were rinsed and incubated with secondary antibody (goat anti-rabbit Alexa Fluor 594) at room temperature for 2 h. Rabbit anti-occludin antibody (abcam, ab222691; and Lectin, Thermofisher, CAT # L32482) was used for blood vessel labelling at a 1:250 dilution in blocking solution. Slides were allowed to dry, mounted with ProLong Gold antifade mountant (P36394) imaged with a Zeiss 710 confocal microscope. We used the Renyi entropy thresholding method to define labelled pixels and calculated the integrated density for each fluorescence channel. Eight fields of view across four slices were averaged for each sample. Results are reported as 'integrated density of occludin/integrated density of lectin'. To determine statistical significance, a two-tailed unpaired *t*-test was performed.

Evans Blue leakage analysis

After the conclusion of 1 week of treatment, the mice in the second cohort were retro-orbitally injected with Evans Blue dye, 2 ml/kg of a 2% solution, to track BBB permeability. One hour after Evans Blue dye injection, they were sacrificed by injection of pentobarbital at 5 mg per 100 g. They were transcardially perfused with 1× PBS followed by 4% PFA. Brains were kept in 4% PFA for 24 h and then transferred to 30% sucrose solution. Brain tissue was cut along the sagittal centreline. Pictures of the half-brains were taken for qualitative analysis.

One hour after an injection of anti-VEGF-A, the mice in cohort 3 were injected with Evans Blue dye, 2 ml/kg of a 2% solution, to track BBB permeability. These mice were similarly sacrificed, but only perfused with 1× PBS. After beheading the mice, the cortex and hippocampus were separated and weighed. The brain sections were then homogenized in a 3:1 PBS:trichloroacetic acid (Sigma-Aldrich) solution to precipitate out macromolecular compounds. Samples were cooled overnight at 4°C and then centrifuged at 1000*g* for 30 min. Evans Blue dye absorbance was quantitatively

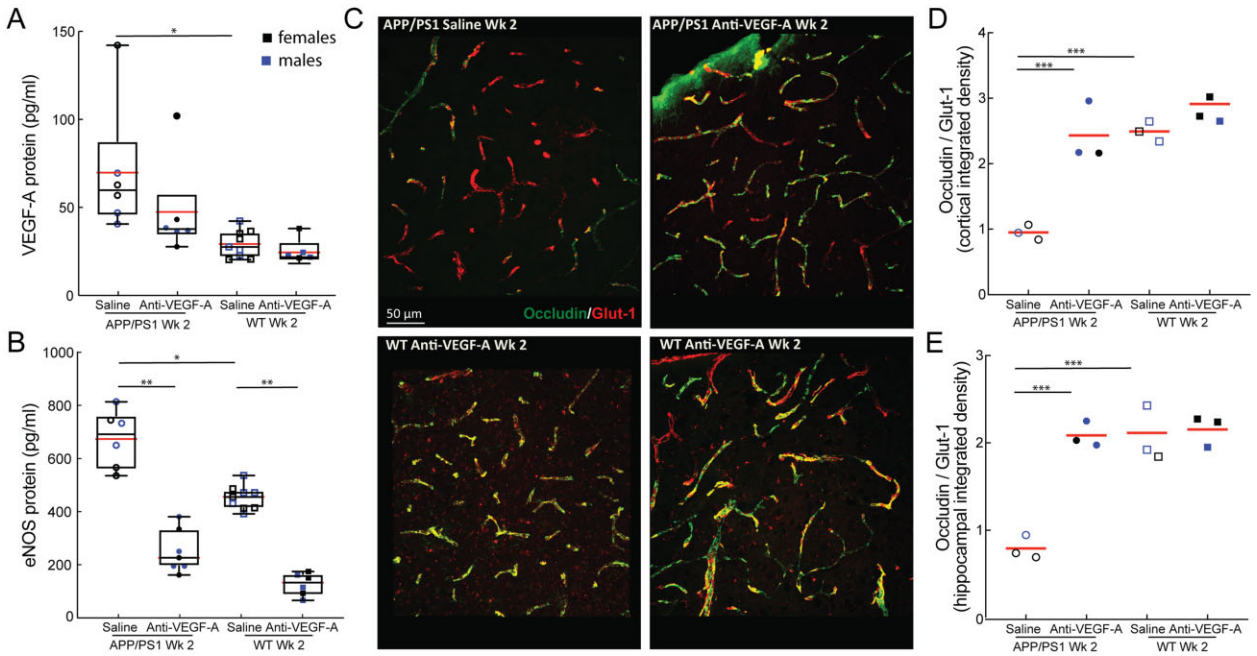

Figure 3 Anti-VEGF-A treatment modulates endothelial protein expression in APP/PS1 mice. ELISA measurements of VEGF-A (**A**) and eNOS (**B**) concentrations after 2 weeks of anti-VEGF-A treatment or saline control injections in APP/PS1 and wild-type (WT) mice (APP/PS1–saline: $n = 6$, APP/PS1–anti-VEGF-A: $n = 6$ (7), WT–saline: $n = 9$, WT--anti-VEGF-A: $n = 5$ (6); one-way ANOVA with Tukey's *post hoc* multiple comparison correction to compare across groups: APP/PS1–saline (VEGF-A) versus APP/PS1–anti-VEGF-A (VEGF-A) $P < 0.075$, WT–saline (VEGF-A) versus WT–anti-VEGF-A (VEGF-A) $P = 0.81$, APP/PS1–saline (VEGF-A) *versus* WT–saline (VEGF-A) $P < 0.05$, APP/PS1–anti-VEGF-A (VEGF-A) versus WT–saline (VEGF-A) $P = 0.93$, APP/PS1–saline (eNOS) versus APP/PS1–anti-VEGF-A (eNOS) $P < 0.01$, WT–saline (eNOS) versus WT–anti-VEGF-A (eNOS) $P < 0.01$, APP/PS1–saline (eNOS) versus WT–saline (eNOS) $P < 0.05$). (**C**) Z-projection of confocal microscopy image stacks from representative cortical areas from mice of all four groups, revealing increased occludin density in anti-VEGF-A-treated APP/PS1 mice as compared to saline-injected APP/PS1 mice. Integrated density of occludin fluorescence as a function of the integrated density of the endothelial cell marker Glut-1 in the cortex (**C**) and hippocampus (**D**) (APP/PS1–saline: $n = 3$, APP/PS1–anti-VEGF-A: $n = 3$, WT–saline: $n = 3$, WT–anti-VEGF-A: $n = 3$; one-way ANOVA with Tukey's *post hoc* multiple comparison correction to compare across groups: APP/PS1–saline cortex versus APP/PS1–anti-VEGF-A cortex $P = 0.0006$, saline WT cortex versus WT–anti-VEGF-A cortex $P = 0.53$, APP/PS1–saline cortex versus WT–saline cortex $P = 0.0005$, APP/PS1–anti-VEGF-A cortex versus WT–saline cortex $P > 0.99$, APP/PS1–saline hippocampus versus APP/PS1–anti-VEGF-A hippocampus $P = 0.0004$, WT–saline hippocampus versus WT–anti-VEGF-A hippocampus $P > 0.99$, APP/PS1–saline hippocampus versus WT–saline hippocampus $P = 0.0002$, APP/PS1–anti-VEGF-A hippocampus versus WT–saline hippocampus $P > 0.99$). Each point represents one mouse and the red horizontal represents the median. Sex differences are indicated by colour, with black data-points representing females and blue representing males.

measured at 620 nm and then divided by the mass of the brain tissue. This methodology has been previously described.[40]

Statistics

The Mann–Whitney *U*-test (two groups) and ANOVA test with Dunn's non-parametric or Tukey's parametric multiple comparison correction (three or more groups) was used to determine statistical differences between groups of data. For longitudinal studies, the ratio paired *t*-test (two groups) or ANOVA repeated-measures option with equal variability of differences (three or more groups) was used. A standard indicator of statistical significance was used throughout the figures ($^{*}P < 0.05$, $^{**}P < 0.01$, $^{***}P < 0.001$, $^{****}P < 0.0001$). If the derived *P*-value was less than 0.05 the difference was considered significant. If the *P*-value was other than such the datasets were assumed to have no difference. Individual data-points are presented in graphical form, with a red line representing the mean. In all graphs, we used different colour data-points to indicate data from male and female mice. Box plot whiskers extend 1.5× the difference between the 25th and 75th percentiles. Longitudinal data are presented in graphs where a solid black line tracks the same mouse over time. Graphpad's Prism 8 software was used for all statistical analyses and graph design.

Data availability

Data associated with this publication will be stored on the Cornell University ecommons server.

Results

Anti-VEGF-A-treated APP/PS1 mice had a reduced incidence of capillary stalls and increased cortical capillary flow speeds

We used *in vivo* 2PEF microscopy to image mouse cortical microvasculature and observed that only 0.3% of capillaries in wild-type mice had obstructed flow (Fig. 1A), whereas 1.5% of capillaries in APP/PS1 mice were stalled (Fig. 1B; Mann Whitney *P*-value < 0.001; Fig. 1D). A majority of the capillaries without flow had leucocytes plugging the vessel lumen (~70%), either with or without one or more RBCs present (Fig. 1E,F). These observations are consistent with our previous findings in APP/PS1 mice, where we demonstrated that 1.8% of capillaries were stalled, leading to reduced blood flow in up- and downstream vessels and causing a 17% reduction in cortical perfusion, as measured by ASL-MRI.[7]

We then inhibited VEGF-A signalling for two weeks by administering anti-VEGF-A antibodies (AF-493, R&D Systems, Inc.; intraperitoneal every other day), and measured the incidence of capillary stalling, capillary blood flow speeds after 1 and 2 weeks

of treatment (Fig. 2A). APP/PS1 mice treated with anti-VEGF-A for 1 and 2 weeks showed reduced incidence of capillary stalls, as compared to saline-treated control (1 week: 1.34% versus 0.44%; 2 weeks: 1.49% versus 0.38%; one-way ANOVA with Holm–Šídák *post hoc* multiple comparison correction; *P*-value = 0.05 and 0.01, respectively; Fig. 2B). In contrast, wild-type mice had low levels of capillary stalls (0.3%) that were not altered by either anti-VEGF-A or saline treatment. Strikingly, anti-VEGF-A-treated APP/PS1 mice had capillary stall incidence that was on par with that of wild-type mice. The anti-VEGF-A-treated APP/PS1 mice also had, on average, 1.5 times faster capillary flow speeds, as compared to saline-treated APP/PS1 mice, after 1 and 2 weeks of treatment (1 week: 2.3 mm/s versus 1.5 mm/s; 2 weeks: 2.4 mm/s versus 1.8 mm/s; one-way ANOVA with Tukey's *post hoc* multiple comparison correction; *P*-value < 0.001 and 0.01, respectively; Fig. 2C and D). Strikingly, the anti-VEGF-A treatment completely eliminated the deficit in capillary flow speeds APP/PS1 mice exhibited relative to wild-type mice. The anti-VEGF-A treatment did not affect capillary flow speeds in wild-type mice (Fig. 2D) or capillary diameter in either APP/PS1 or wild-type mice (Fig. 2E).

Anti-VEGF-A-treated APP/PS1 mice had reduced eNOS and increased occludin levels

After *in vivo* imaging, the mice were euthanized and their brain tissue was processed for measuring protein concentration and histology. The anti-VEGF-A treatment lowered the concentration of VEGF-A in whole-brain extracts from APP/PS1 mice by 50%, as measured by ELISA and compared to saline-treated APP/PS1 mice, which brought the VEGF-A concentration in line with that from saline-treated wild-type mice (Fig. 3A). eNOS was reduced by 70% with anti-VEGF-A treatment in APP/PS1 mice, as measured by ELISA and compared to saline treatment (Fig. 3B). A similar fractional reduction in eNOS was observed in wild-type mice treated with anti-VEGF-A. Saline-treated APP/PS1 mice had ∼1.5 times higher eNOS concentrations than saline-treated wild-type mice. In histological sections, we quantified the expression of occludin in capillaries from the cortex and hippocampus (Fig. 3C). Anti-VEGF-A treatment of APP/PS1 mice increased occludin concentration by 2.5 and 2.0 times in the cortex and hippocampus, respectively, as compared to saline treatment, bringing occludin concentration to the same level as in wild-type mice (Fig. 3D and E). We also measured protein levels of the VEGF 1 and 2 receptors from brain and plasma samples. There was an overall lower concentration of VEGF1R receptors in brain lysates in Alzheimer's disease as compared to wild-type mice, but no notable change with anti-VEGF treatment after 1 week of treatment (Supplementary Fig. 2A). In contrast, there were higher concentrations of VEGF2R levels in APP/PS1 mice compared to wild-type mice and a trend towards reduced VEGF2R protein levels in APP/PS1 mice after anti-VEGF treatment (Supplementary Fig. 2B). Next, we tested for the soluble forms of these two receptors from plasma samples, but did not detect any differences between APP/PS1 mice and wild-type mice or between anti-VEGF-treated mice and saline-injected (Supplementary Fig. 2C and D). In addition, 2 weeks of anti-VEGF-A treatment did not change the levels of soluble amyloid-β_{40}, non-soluble amyloid-β_{40}, soluble amyloid-β_{42}, or non-soluble amyloid-β_{42} in APP/PS1 mice (Supplementary Fig. 3).

Consistently stalled capillaries showed lower occludin expression in anti-VEGF-A-treated APP/PS1 mice

To further explore the potential link between occludin expression and capillary stalling, we sought to correlate these on a capillary-by-capillary basis. In the anti-VEGF-A-treated APP/PS1 mice, there were some capillaries that we observed to stall in the last imaging session (Fig. 4A). In a total of five mice we were able to spatially align sagittal brain sections with the *in vivo* imaging by manually matching the patterns of the capillaries imaged *in vivo* with those labelled by post-mortem occludin staining (Fig. 4B and C). Using this approach, we were able to unambiguously identify 10 capillaries that were stalled on the last imaging session in the occluding-stained sections. We further identified 100 capillaries that were flowing. We quantified the average intensity of occludin staining along identified capillaries and found that the stalled capillaries had ∼40% lower occludin expression than the flowing capillaries in both anti-VEGF- and saline-treated APP/PS1 mice (Fig. 4D; Mann–Whitney anti-VEGF *P*-value < 0.0001, saline *P*-value < 0.001). The very low number of stalled capillaries in the anti-VEGF-A-treated APP/PS1 mice coupled with the experimental challenge of unambiguously matching individual capillaries across the *in vivo* and post-mortem images precluded us from increasing the number of stalled capillaries that were analysed.

Anti-VEGF-A treatment reduced capillary stalls and increased capillary blood flow speed in APP/PS1 mice within an hour of injection

VEGF-A signalling can rapidly change the incorporation of tight junction proteins, such as occludin, at the BBB on a ∼15-min timescale, altering BBB permeability.[41] We tested whether the impact of anti-VEGF-A on the incidence of capillary stalls in APP/PS1 mice was similarly fast (Fig. 5A). We found that 1 h after a single anti-VEGF-A injection, APP/PS1 mice had 59% fewer capillary stalls (0.5%) than at baseline (1.2%; repeated-measures one-way ANOVA with Tukey's *post hoc* multiple comparison correction; *P*-value < 0.02; Fig. 5B–D). We continued giving anti-VEGF-A every other day for a week, and found that stall incidence remained low, consistent with the data in Fig. 2. Wild-type mice had low stall incidence both before and after anti-VEGF-A treatment (Fig. 5D). At baseline, APP/PS1 mice had 25% slower capillary flow speeds, as measured with line scans (Fig. 5E), as compared to wild-type mice. The rapid reduction in capillary stalls in APP/PS1 mice with anti-VEGF-A treatment was associated with a 20% on average, increase in capillary blood flow speed (vessels < 10 μm), at 1 h after injection and was maintained at 1 week (Fig. 5F). We did not observe differences in capillary diameter between groups, nor did we detect significant changes in capillary diameter with anti-VEGF-A treatment (Fig. 5G).

Anti-VEGF-A treatment reduced BBB permeability in APP/PS1 mice within an hour of injection

Consistent with the known BBB tightening effects of anti-VEGF-A treatment, we observed reduced staining of the brain with intravascularly circulating Evans Blue dye when these animals were sacrificed (Fig. 6A). In summary, anti-VEGF-A treatment reduced capillary stalls and increased capillary blood flow speeds in APP/PS1 mice within 1 h, bringing both to the levels of wild-type mice. We measured BBB permeability by quantifying the amount of intravenously circulating Evans Blue dye found in post-mortem, perfused brain tissue (Fig. 6B). APP/PS1 mice treated with anti-VEGF-A 1 h before injecting Evans Blue had half of the dye concentration in the cortex and hippocampus as compared to APP/PS1 mice treated with saline (one-way ANOVA with Tukey's *post hoc* multiple comparison correction; *P*-value < 0.01; Fig. 6C and D, respectively), which suggests that anti-VEGF treatment improved the BBB permeability of APP/PS1 mice to a similar level to that of wild-type mice.

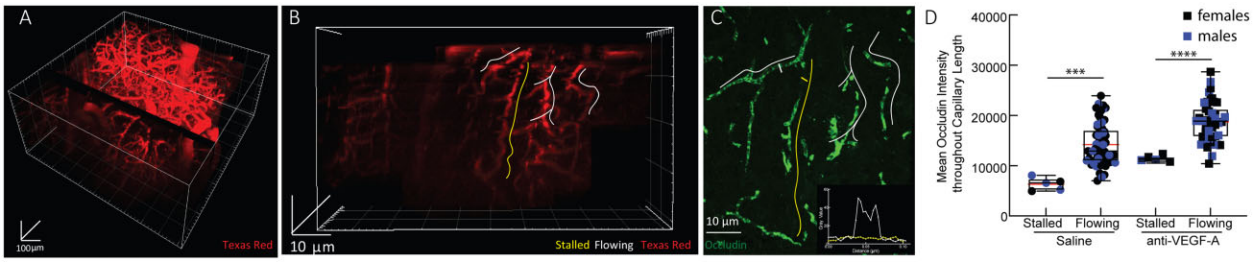

Figure 4 Anti-VEGF-A-treated APP/PS1 mice had lower occludin expression in stalled capillaries as compared to flowing capillaries. Capillaries of APP/PS1 mice treated with anti-VEGF-A seen via *in vivo* 2PEF imaging (**A** and **B**), with flowing (white highlight) and stalled (yellow highlighted) vessels indicated, spatially aligned to occludin immunofluorescence histopathology (**C**) revealing lower occludin fluorescence at stalled capillaries as compared to flowing capillaries. The inset graph in the lower right tracks the cross-sectional mean grey value of occludin fluorescence across the distance of the white and yellow dashes on the stalled and flowing capillary. (**D**) Mean occludin concentrations, determined from the immunohistochemistry, for flowing and capillary segments, determined from *in vivo* imaging, in APP/PS1 mice treated with anti-VEGF-A for 2 weeks (APP/PS1 saline $n = 3$ mice, 61 capillaries and APP/PS1 anti-VEGF-A $n = 2$ mice, 43 capillaries; Kruskal–Wallis test with multiple comparison correction to compare across groups; saline P-value < 0.001, anti-VEGF-A $P < 0.0001$); bar graph represents mean values, and error bars represent standard deviation). Sex differences are indicated by colour, with black data-points representing females and blue representing males.

Anti-VEGF-A treatment reduced capillary density in APP/PS1 mice after a week of chronic treatment

Finally, we probed whether the anti-VEGF-A treatment was associated with differences in cortical capillary density. We used DeepVess, a convolutional neural network-based segmentation algorithm, to segment 3D image stacks of the cortical microvasculature (excluding larger surface blood vessels) and quantified the fraction of image voxels that were within vessels to measure capillary density (Supplementary Fig. 4A–C). APP/PS1 mice had a 20% higher capillary density than wild-type mice at baseline. After 1 week of anti-VEGF-A treatment the capillary density trended towards a reduction in the APP/PS1 mice, with this result just short of significance (8% reduction, $P = 0.07$). Anti-VEGF-A treatment was not associated with capillary density differences in wild-type mice (Supplementary Fig. 4C).

Occludin level was reduced in patients with Alzheimer's disease

Immunofluorescence of cortical tissue from Alzheimer's disease patients and healthy controls demonstrated decreased occludin expression in the Alzheimer's disease brain microvasculature (Fig. 7A and B and Supplementary Table 1), similar to what we found in APP/PS1 mice.

Discussion

CBF reductions occur in most dementia patients and are associated with cognitive impairment in cross-sectional studies.[42] Such CBF reductions develop early in the pathogenesis of Alzheimer's disease, when intervention would be most ideal.[43] We previously showed that a small fraction of cortical capillaries is temporarily stalled at a four times higher rate in multiple mouse models of APP overexpression, as compared to wild-type mice.[35,42,44] Furthermore, we found that administering an antibody against a neutrophil-specific protein, Ly6G, led to a ~64% reduction in the incidence of capillary stalling and a ~17% increase in CBF. This was associated with rapid improvements in short-term memory in APP/PS1 mice as old as 16 months of age.[7,45] In this study we demonstrate that inhibition of VEGF-A signalling normalizes aberrant eNOS/occludin-associated BBB permeability, increases in capillary stalls, and reductions in CBF (Supplementary Fig. 5).

A recent study followed the fate of capillaries with long-lived (>20 min) spontaneous or injected-microsphere-induced obstructions in wild-type mice, and found that obstructed capillaries were prone to being pruned from the vascular network, but that both obstructions and pruning were markedly decreased when VEGF-receptor 2 (the dominant VEGF-A receptor in endothelial cells[46]) signalling was blocked.[17] Several studies have explored the role of VEGF-A signalling in patients with Alzheimer's disease. Many studies find increased levels of VEGF-A in the serum or CSF of patients with Alzheimer's disease,[19,47–49] with others showing reduced[23,50] or unchanged levels.[51,52] Increased VEGF-A levels are also seen in brain homogenates from the TgCNDR8[53] and APP/PS1 mouse models of Alzheimer's disease,[54] as well as in endothelial cells of arteries, veins and capillaries from aged wild-type mice,[55] mouse models of APP overexpression,[27,54] mutant Tau mice[56] and patients with Alzheimer's disease.[57–59] However, decreased capillary VEGF-A expression levels have also been found in patients with Alzheimer's disease using single-cell sequencing[52] and immunohistochemistry.[28] Despite the complexity and confusion about baseline changes in VEGF signalling in Alzheimer's disease patients and animal models, our work here demonstrates that inhibiting VEGF signalling ameliorates capillary stalling and CBF reductions in APP/PS1 mice.

We showed that a 2-week treatment of intraperitoneally injected anti-VEGF-A reduced the number of capillary stalls and increased capillary RBC flow speeds in APP/PS1 mice and that this was accompanied by a tightening of the BBB. We tested for sex differences and identified a non-significant trend towards increased capillary stalls in APP/PS1 female mice, as compared to males. Interestingly it has been shown that VEGF-A levels are higher in females compared to males, which could contribute to the higher capillary stall rates.[60] Several cellular mechanisms are known to link VEGF signalling to BBB permeability and these mechanisms may play a role in the inhibition of capillary stalling with anti-VEGF treatment. Luminal VEGF-A signalling upregulates enzymes, including the endothelial isoform of nitric oxide synthase (eNOS), that increase vascular permeability, allowing for the endothelial cell rearrangements that support sprouting angiogenesis.[61] The eNOS upregulation leads to decreased expression and modifications of several tight junction (TJ) proteins, including occludin.[62] Decreased occludin levels are associated with increased BBB permeability[63,64] and decreased TJ complex pore formation.[65] In addition, eNOS knockout mice show increased levels of TJ proteins including occludin and have decreased BBB permeability.[66] Here, we found increased eNOS and decreased occludin expression in APP/PS1 mice, which was rescued with anti-VEGF treatment. Moreover, in a select dataset that correlated *in vivo* stalls with post-mortem protein expression, we also showed that occludin

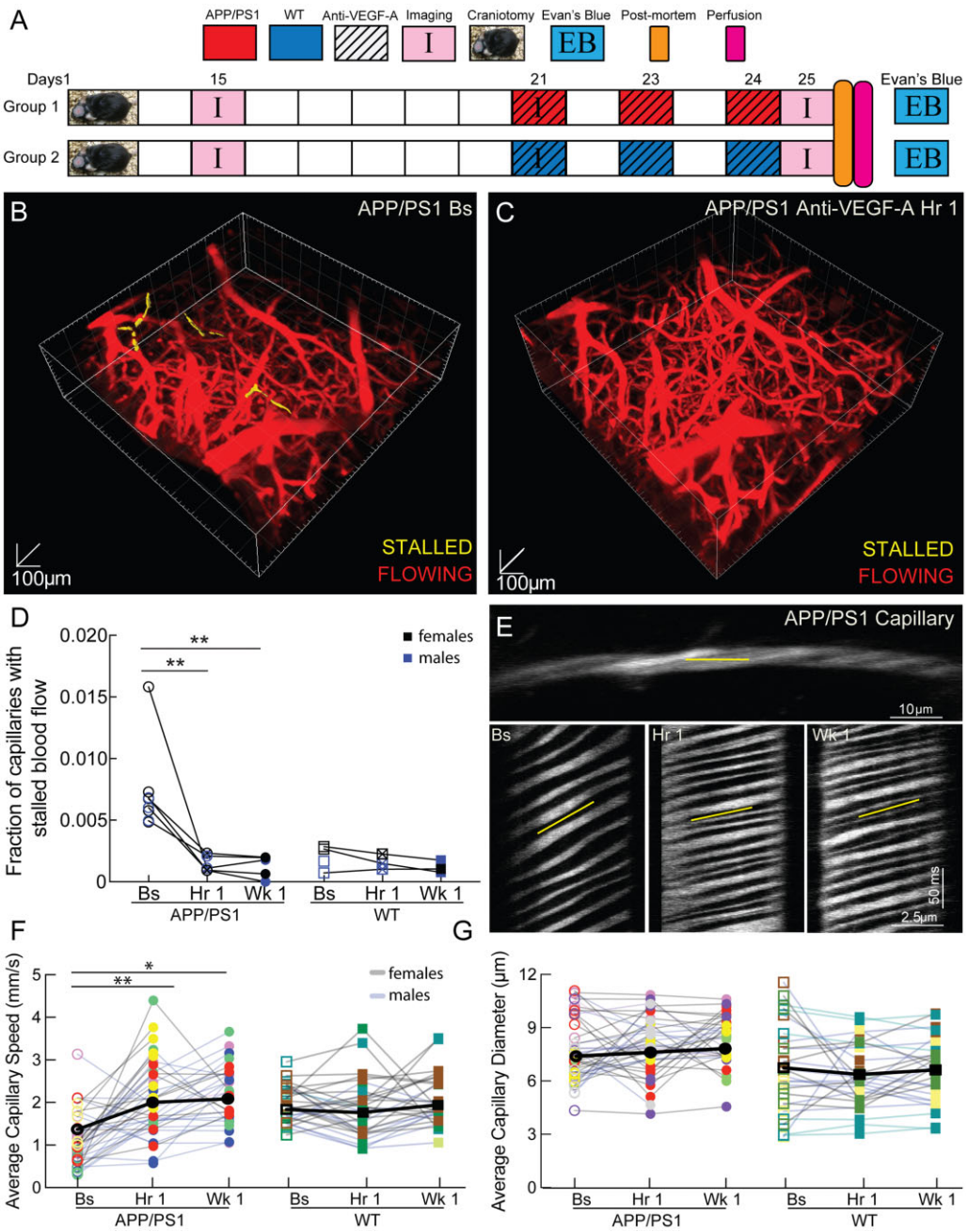

Figure 5 Anti-VEGF-A antibody treatment reduced capillary stalls and increased capillary flow speed within 1 h in APP/PS1 mice. (**A**) Schematic of experimental timeline. Craniotomies were performed on APP/PS1 mice and they recovered for 2 weeks. The mice were divided into two groups: APP/PS1 mice treated with anti-VEGF-A ($n = 9$; APP/PS1–anti-VEGF-A) and wild-type (WT) mice treated with anti-VEGF-A ($n = 4$; WT–anti-VEGF-A). These mice were imaged three times—twice on the first imaging day before and ∼1 h after treatment and again 5 days later after two additional treatments. The brains were harvested for post-mortem assays after the second imaging session. Rendering of 2PEF stacks of the brain from the same APP/PS1 mouse before (**B**) and 1 h after (**C**) anti-VEGF-A injection. Capillaries that were stalled are highlighted in yellow. (**D**) The fraction of capillaries with stalled blood flow at baseline (Bs), 1 h after anti-VEGF-A injection and after 1 week of treatment in APP/PS1 and WT mice (APP/PS1: 4 mice could not be imaged at 1 week due to window loss or death; ∼60 000 capillaries; repeated-measures one-way ANOVA with Tukey's *post hoc* multiple comparison correction to compare baseline to 1 h and 1 week: APP/PS1–baseline versus APP/PS1–1-h $P = 0.02$, APP/PS1–baseline versus APP/PS1–1-week $P = 0.005$; Kruskal–Wallis test with multiple comparison correction to compare across groups; each data-point in the graph represents the capillaries with stalled blood flow as a function of total capillaries in 4–6 2PEF stacks for each mouse). Sex differences are indicated by colour, with black data-points representing females and blue representing males. (**E**) Image (*top*) and line scans (*bottom*) from a representative capillary from an APP/PS1 mouse taken at baseline and at 1 h and 1 week after anti-VEGF-A treatment, showing higher RBC flow speeds after treatment. (**F**) Average RBC flow speed and (**G**) vessel diameter from cortical capillaries at baseline and at 1 h and 1 week after anti-VEGF-A injection in APP/PS1 and WT mice (APP/PS1–baseline: $n = 9$, 53 capillaries, APP/PS1–1-h: $n = 6$ (one mouse died, two mice lost cranial windows), 45 capillaries, APP/PS1–1-week: $n = 5$ (one mouse lost cranial window), 35 capillaries, WT–baseline: $n = 4$, 21 capillaries, WT–1-h: $n = 3$ (one mouse lost cranial window), 23 capillaries, WT–1-week: $n = 3$, 21 capillaries; repeated-measures one-way ANOVA with Tukey's *post hoc* multiple comparison correction to compare baseline to 1 h to 1 week: APP/PS1–baseline versus APP/PS1–1-h $P = 0.0100$, APP/PS1–baseline versus APP/PS1–1-week $P = 0.0288$, WT–baseline versus WT–1-h $P = 0.9390$, WT–baseline versus WT–1-week $P = 0.2884$). In all graphs, lines connecting data-points represent the same capillary, while different colours represent individual mice. Sex differences are indicated by colour, with shaded black lines between the data-points representing females and shaded blue lines between data-points representing males.

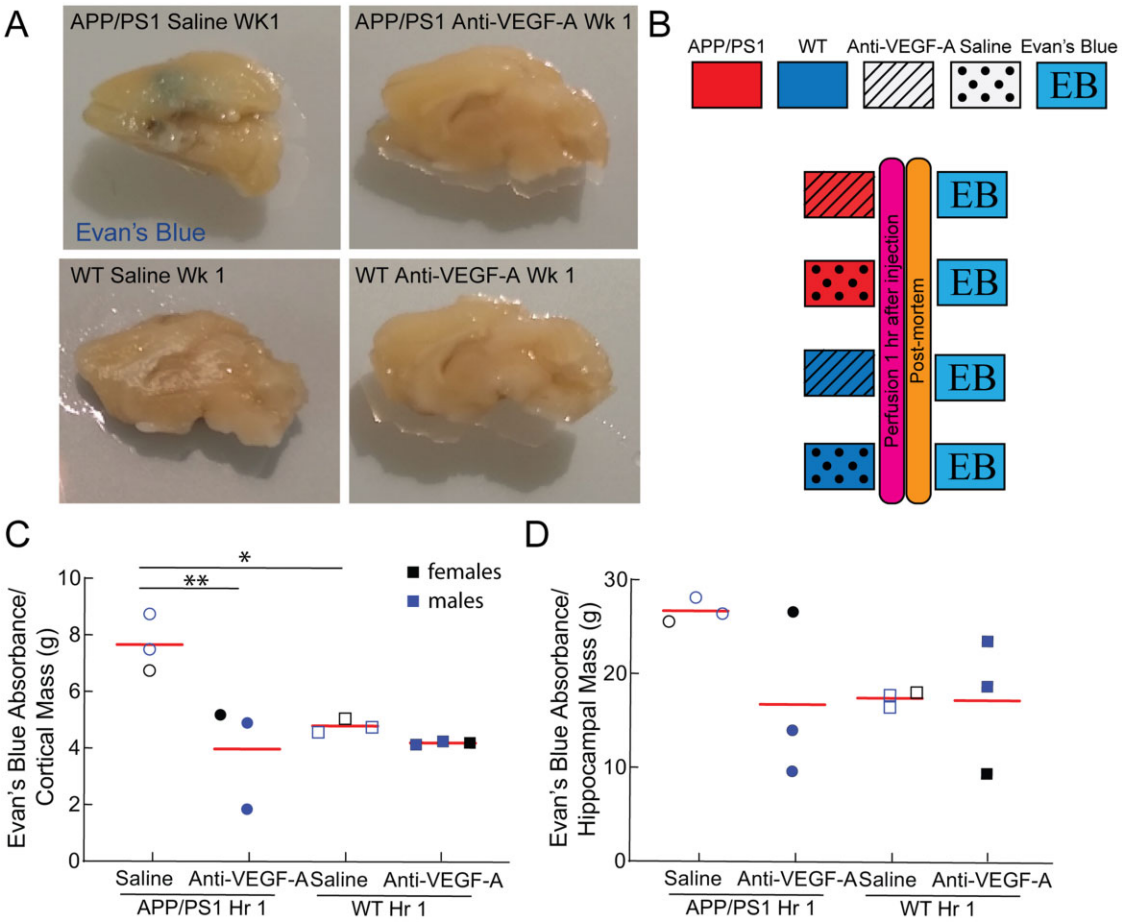

Figure 6 Anti-VEGF-A antibody treatment reduces BBB leakage within 1 h in APP/PS1 mouse. (**A**) Sagittally cut brain slices from APP/PS1 and wild-type (WT) mice treated with anti-VEGF-A or saline for 1 week and after 1 h of intravenous circulation of Evans Blue dye. Arrow indicates region of increased penetration of Evans Blue into the brain in the APP/PS1 saline-treated mouse. (**B**) Schematic of experimental timeline. APP/PS1 and WT mice were treated with anti-VEGF-A or saline. Evans Blue was intravenously injected an hour before perfusion and the extent of Evans Blue entry into the brain from the vasculature was quantified ($n = 3$ mice per group). Normalized absorbance of whole cortex (**C**) or hippocampus (**D**) tissue homogenates at 620 nm, to quantify the extent of Evans Blue entry into the brain for APP/PS1 and WT mice treated with anti-VEGF-A or saline (one-way ANOVA with Tukey's *post hoc* multiple comparison correction: **C**, saline APP/PS1 versus anti-VEGF-A APP/PS1 $P = 0.01$; **C**, saline APP/PS1 versus saline WT $P = 0.04$). In the graphs each point represents data from one mouse and the red horizontal line represents the mean. Sex differences are indicated by colour, with black data-points representing females and blue representing males.

levels are reduced specifically in stalled capillaries, further strengthening this correlation. This finding is consistent with previous results showing decreased occludin expression in Alzheimer's disease mouse models, including the APP/PS1 model,[26,67] and in the cortex of Alzheimer's disease patients,[68,69] which we replicated here. The overall strong reduction in VEGF-A protein in brain lysates after 2 weeks of anti-VEGF-A antibody treatment also suggests that other VEGF-dependent signalling pathways in endothelial and other brain cells are likely altered and could contribute to the modulation of capillary stalling.

We also observed very fast effects on capillary stalling and CBF with anti-VEGF-A treatment in APP/PS1 mice, with these rapid changes in capillary stalling and CBF of the same magnitude as those seen with 1–2 weeks of anti-VEGF-A administration. The rapid changes in capillary stalling were, again, correlated with decreased BBB permeability. Interestingly, increases in the phosphorylation status of occludin are implicated in decreased BBB permeability that occurs within minutes of inhibiting VEGF-A signalling.[41,70,71] It seems likely that such post-translational modifications similarly contribute to the rapid changes in capillary stalling seen here. Other downstream effects of VEGF signalling, such as angiogenesis,[8] vascularization,[9] lymphangiogenesis,[10] growth tip guidance,[11] neurogenesis[11] and neuroprotection, are less likely occurring at this rapid timescale, further implicating loss of BBB integrity and hyperpermeability in the formation of capillary stalls. Indeed, changes in capillary density were only seen after 1 week of anti-VEGF therapy among APP/PS1 mice.

An analogy supporting these ideas has been suggested in the retina. Several studies have analyzed the role of VEGF-A signalling in the blood–retina barrier permeability in diabetic retinopathy and have shown that intravitreal injections of anti-VEGF-A lead to an increase in occludin phosphorylation and tightening of the blood–retina barrier within hours that was correlated with a reduction in the incidence of leucocytes stuck in retinal microvessels.[71–74] In diabetic retinopathy inhibition of the vascular inflammatory receptor ICAM-1 leads to reduced leucostasis and vascular leakage[75] and VEGF-A leads to increased levels of ICAM-1 in the vasculature.[76] In Alzheimer's disease, low-level chronic vascular inflammation is also present.[77] This is supported by recent single-nucleus transcriptome analysis of endothelial cells, which have shown an increased level of genes involved in vascular inflammation in aged healthy humans[55] and patients with Alzheimer's disease.[58] The functional consequences of increased chronic vascular inflammation have also been studied. For example, mouse models of Alzheimer's disease have

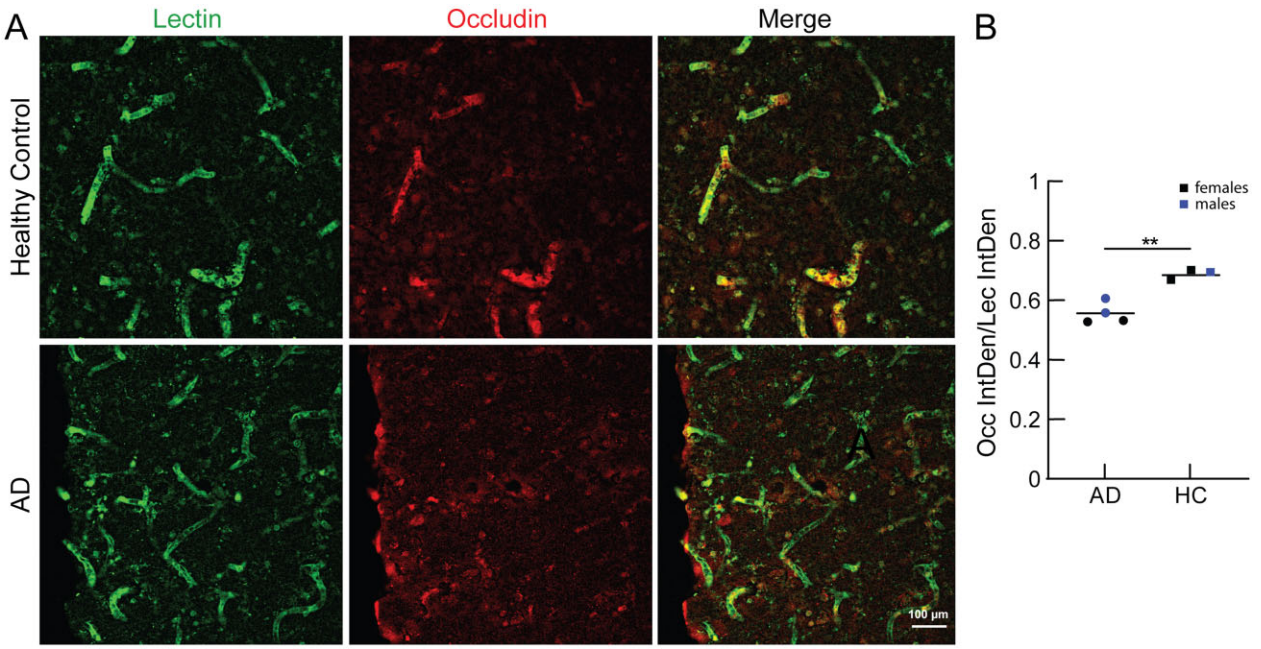

Figure 7 Occludin staining in cortical brain sections from Alzheimer's disease patients and healthy controls. (**A**) Z-projection of confocal microscopy image stacks from representative cortical areas from healthy controls (*top*) and Alzheimer's disease patients (*bottom*), revealing reduced occludin levels (red) in cortical capillaries identified by lectin staining (green). (**B**) Integrated density of occludin fluorescence, normalized to that of lectin. Eight fields of view from four sections were averaged for each sample (healthy controls $n = 3$ and Alzheimer's disease patients $n = 4$; two-tailed unpaired *t*-test, $^{**}P = 0.01$; red horizontal line represents the median). Sex differences are indicated by colour, with black data-points representing females and blue representing males.

increased endothelia/leucocyte interactions due to increased inflammation and the presence of neutrophil extracellular traps.[78–80] Ultimately, this chronic vascular inflammation could directly increase the number of capillary stalls and impact CBF. Overall these data indicates that luminal VEGF-A signalling plays a highly complex role in regulating endothelial function in the APP/PS1 mouse.

VEGF plays a role in a wide variety of signalling pathways and can act both on endothelial cells (luminal) and brain cells (parenchymal). VEGF-A and its receptors are expressed by all brain cell-types[81,82] and likely impact pathways and cell–cell interactions beyond those considered in this study. In fact, the large reduction in VEGF-A levels after anti-VEGF-A treatment we found suggests many signalling mechanisms are likely altered. VEGF levels and signalling response may also depend on additional factors such as sex, disease stage, or cardiovascular risk factors, for example. Alterations of VEGF signalling in different tissue compartments of the brain and in the periphery could have different impacts on downstream aspects of Alzheimer's disease, such as cognition.[83] In this study, we measured increased levels of VEGF-A in APP/PS1 mice from brain lysates. Unfortunately, we could not separate our analysis into cell types—endothelial, neuronal, or glial—due to a lack of raw material. This study has linked peripheral VEGF-A signalling to increased rates of capillary stalling and CBF reductions in the APP/PS1 mouse model of Alzheimer's disease. However, VEGF-A is a multifactorial signalling molecule and has various functions in different cell types. For example, VEGF-A supplementation led to improved short-term memory in mouse models of Alzheimer's disease.[84] The injection of bone marrow-derived mesenchymal stem cells expressing the human VEGF-A165 isoform led to cognitive improvements in the plus-maze discriminative avoidance task, reduced parenchymal amyloid plaques and initiated neovascularization.[85] Similar results were seen in mice overexpressing the human VEGF-A165 in neurons in mouse models of Alzheimer's disease.[84,86] Overall this sounds contradictory, but we show that reducing peripheral levels of VEGF-A increases BBB integrity and improves CBF, while others show overexpressed neuronal VEGF-A via stem cells transplantation leads to improvements of Alzheimer's disease-related pathology. However, this could simply mean that increased VEGF-A signalling may be protective to the CNS on one side of the BBB and that it may contribute to mechanisms within the vasculature that enhance the impact of Alzheimer's disease pathology. Unifying these hypotheses suggests that increased levels of peripheral VEGF is a compensatory mechanism in response to reduced signalling in the brain. The idea that VEGF-A is still produced but the signalling is impaired has been proposed as pathological angiogenesis in Alzheimer's disease.[87] Furthermore, this hypothesis is also supported by the fact that large molecules, including IgG immunoglobulins (molecular weight = 150 kDa), have a less than 1 in 1000 probability to cross the BBB,[30,32] even in BBB impaired models such as the APP/PS1 model.[88] This suggests that the anti-VEGF-A 165 antibody disproportionally inhibits luminal rather than parenchymal VEGF-A signalling, especially for the short-timescale experiments that demonstrated correlated decreases in capillary stalling and BBB permeability 1 h after anti-VEGF-A treatment.

In summary, this study describes how peripherally inhibiting VEGF-A signalling in APP/PS1 mice leads to increased BBB integrity, which correlates with decreased capillary stalling and increased CBF. Furthermore, it describes how increased non-functional, pro-angiogenic VEGF-A signalling seen in Alzheimer's disease could contribute to reduced CBF likely via capillary stalls. Given the complex role of VEGF signalling in Alzheimer's disease, caution is warranted in contemplating the clinical implications of our findings. However, acute treatment with anti-VEGF, coupled with brain blood flow measurements could be a path to assessing whether capillary stalls may contribute to reduced CBF in patients with Alzheimer's disease.

Acknowledgements

We want to thank Mike Lamont for developing the DeepVess editor app. Confocal imaging data were acquired through the Cornell University Biotechnology Resource Center, with NIH funding (grant number RR025502) for the shared Zeiss LSM 710 Confocal. Human brain tissue was provided by the NIH NeuroBioBank, the Harvard Brain Tissue Resource Center, Sepulveda Research Corporation, the Mount Sinai/JJ Peters VA Medical Center NIH Brain and Tissue Repository and the University of Maryland Brain and Tissue Bank. A list of individual Stall Catchers contributors who contributed to this study is at https://humancomputation.org/sc-vegf/

Funding

This research was supported by the German National Academic Scholarship Foundation (K.F.), the National Institutes of Health grants AG049952 (C.B.S.) and NS108472 (C.B.S.), the BrightFocus Foundation (C.B.S.) and by the DFG German Research Foundation (O.B.).

Competing interests

The authors report no competing interests.

Supplementary material

Supplementary material is available at *Brain* online.

References

1. Santos CY, Snyder PJ, Wu WC, Zhang M, Echeverria A, Alber J. Pathophysiologic relationship between Alzheimer's disease, cerebrovascular disease, and cardiovascular risk: A review and synthesis. *Alzheimers Dement (Amst)*. 2017;7:69–87.
2. Dai W, Lopez OL, Carmichael OT, Becker JT, Kuller LH, Gach HM. Mild cognitive impairment and Alzheimer disease: Patterns of altered cerebral blood flow at MR imaging. *Radiology*. 2009; 250(3):856–866.
3. Bracko O, Cruz Hernández JC, Park L, Nishimura N, Schaffer CB. Causes and consequences of baseline cerebral blood flow reductions in Alzheimer's disease. *J Cereb Blood Flow Metab*. 2021;41(7):1501–1516.
4. Wiesmann M, Zerbi V, Jansen D, et al. Hypertension, cerebrovascular impairment, and cognitive decline in aged AbetaPP/PS1 mice. *Theranostics*. 2017;7(5):1277–1289.
5. Nation DA, Wierenga CE, Clark LR, et al. Cortical and subcortical cerebrovascular resistance index in mild cognitive impairment and Alzheimer's disease. *J Alzheimers Dis*. 2013;36(4):689–698.
6. Heo S, Prakash RS, Voss MW, et al. Resting hippocampal blood flow, spatial memory and aging. *Brain Res*. 2010;1315:119–127.
7. Hernandez, JC Bracko, O Kersbergen, CJ, et al. Neutrophil adhesion in brain capillaries reduces cortical blood flow and impairs memory function in Alzheimer's disease mouse models. *Nat Neurosci*. 2019;22(3):413–420.
8. Vezzani A. VEGF as a target for neuroprotection. *Epilepsy Curr*. 2008;8(5):135–137.
9. Pandey AK, Singhi EK, Arroyo JP, et al. Mechanisms of VEGF (vascular endothelial growth factor) inhibitor-associated hypertension and vascular disease. *Hypertension*. 2018;71(2):e1–e8.
10. Kinashi H, Ito Y, Sun T, Katsuno T, Takei Y. Roles of the TGF-beta(-)VEGF-C pathway in fibrosis-related lymphangiogenesis. *Int J Mol Sci*. 2018;19(9):2487.
11. Gerhardt H, Golding M, Fruttiger M, et al. VEGF guides angiogenic sprouting utilizing endothelial tip cell filopodia. *J Cell Biol*. 2003;161(6):1163–1177.
12. Dela Paz NG, Walshe TE, Leach LL, Saint-Geniez M, D'Amore PA. Role of shear-stress-induced VEGF expression in endothelial cell survival. *J Cell Sci*. 2012;125(Pt 4):831–843.
13. Jiang S, Xia R, Jiang Y, Wang L, Gao F. Vascular endothelial growth factors enhance the permeability of the mouse blood–brain barrier. *PLoS One*. 2014;9(2):e86407.
14. Bates DO. Vascular endothelial growth factors and vascular permeability. *Cardiovasc Res*. 2010;87(2):262–271.
15. Suzuki Y, Nagai N, Umemura K. A review of the mechanisms of blood–brain barrier permeability by tissue-type plasminogen activator treatment for cerebral ischemia. *Front Cell Neurosci*. 2016;10:2.
16. Joussen AM, Poulaki V, Qin W, et al. Retinal vascular endothelial growth factor induces intercellular adhesion molecule-1 and endothelial nitric oxide synthase expression and initiates early diabetic retinal leukocyte adhesion *in vivo*. *Am J Pathol*. 2002; 160(2):501–509.
17. Reeson P, Choi K, Brown CE. VEGF signalling regulates the fate of obstructed capillaries in mouse cortex. *Elife*. 2018;7:e33670.
18. Schager B, Brown CE. Susceptibility to capillary plugging can predict brain region specific vessel loss with aging. *J Cereb Blood Flow Metab*. 2020;40(12):2475–2490.
19. Tarkowski E, Issa R, Sjogren M, et al. Increased intrathecal levels of the angiogenic factors VEGF and TGF-beta in Alzheimer's disease and vascular dementia. *Neurobiol Aging*. Mar–Apr 2002; 23(2):237–243.
20. Kim YN, Kim DH. Decreased serum angiogenin level in Alzheimer's disease. *Prog Neuropsychopharmacol Biol Psychiatry*. 2012;38(2):116–120.
21. Thomas T, Miners S, Love S. Post-mortem assessment of hypoperfusion of cerebral cortex in Alzheimer's disease and vascular dementia. *Brain*. 2015;138(Pt 4):1059–1069.
22. Yu S, Liu YP, Liu YH, et al. Diagnostic utility of VEGF and soluble CD40L levels in serum of Alzheimer's patients. *Clin Chim Acta*. 2016;453:154–159.
23. Mateo I, Llorca J, Infante J, et al. Low serum VEGF levels are associated with Alzheimer's disease. *Acta Neurol Scand*. 2007;116(1): 56–58.
24. Huang L, Jia J, Liu R. Decreased serum levels of the angiogenic factors VEGF and TGF-β1 in Alzheimer's disease and amnestic mild cognitive impairment. *Neurosci Lett*. 2013;550:60–63.
25. Malashenkova IK, Hailov NA, Krynskiy SA, et al. [Levels of proinflammatory cytokines and vascular endothelial growth factor in patients with Alzheimer's disease and mild cognitive impairment]. *Zh Nevrol Psikhiatr Im S S Korsakova*. 2016;116(3): 39–43.
26. Provias J, Jeynes B. Correlation analysis of capillary APOE, VEGF and eNOS expression in Alzheimer brains. *Curr Alzheimer Res*. 2011;8(2):197–202.
27. Thirumangalakudi L, Samany PG, Owoso A, Wiskar B, Grammas P. Angiogenic proteins are expressed by brain blood vessels in Alzheimer's disease. *J Alzheimers Dis*. 2006;10(1):111–118.
28. Provias J, Jeynes B. Reduction in vascular endothelial growth factor expression in the superior temporal, hippocampal, and brainstem regions in Alzheimer's disease. *Curr Neurovasc Res*. 2014;11(3):202–209.
29. Herrán E, Pérez-González R, Igartua M, Pedraz JL, Carro E, Hernández RM. VEGF-releasing biodegradable nanospheres administered by craniotomy: Novel therapeutic approach in the APP/Ps1 mouse model of Alzheimer's disease. *J Control Release*. 2013;170(1):111–119.

30. Atwal JK, Chen Y, Chiu C, et al. A therapeutic antibody targeting BACE1 inhibits amyloid-beta production *in vivo*. *Sci Transl Med*. 2011;3(84):84ra43.
31. Tabrizi M, Bornstein GG, Suria H. Biodistribution mechanisms of therapeutic monoclonal antibodies in health and disease. *AAPS J*. 2010;12(1):33–43.
32. Yu YJ, Zhang Y, Kenrick M, et al. Boosting brain uptake of a therapeutic antibody by reducing its affinity for a transcytosis target. *Sci Transl Med*. 2011;3(84):84ra44.
33. Pologruto TA, Sabatini BL, Svoboda K. ScanImage: Flexible software for operating laser scanning microscopes. *Biomed Eng*. 2003;2:13.
34. Santisakultarm TP, Cornelius NR, Nishimura N, et al. *In vivo* two-photon excited fluorescence microscopy reveals cardiac- and respiration-dependent pulsatile blood flow in cortical blood vessels in mice. *Am J Physiol Heart Circ Physiol*. 2012;302(7): H1367–H1377.
35. Bracko O, Vinarcsik LKC, Hernandez, JC, et al. High fat diet worsens Alzheimer's disease-related behavioral abnormalities and neuropathology in APP/PS1 mice, but not by synergistically decreasing cerebral blood flow. *Sci Rep*. 2020;10(1):9884.
36. Haft-Javaherian M, Fang L, Muse V, Schaffer CB, Nishimura N, Sabuncu MR. Deep convolutional neural networks for segmenting 3D *in vivo* multiphoton images of vasculature in Alzheimer disease mouse models. *PLoS One*. 2019;14(3):e0213539.
37. Tariq S, Barber PA. Dementia risk and prevention by targeting modifiable vascular risk factors. *J Neurochem*. 2018;144(5): 565–581.
38. Santisakultarm TP, Paduano CQ, Stokol T, et al. Stalled cerebral capillary blood flow in mouse models of essential thrombocythemia and polycythemia vera revealed by *in vivo* two-photon imaging. *J Thromb Haemost*. 2014;12(12):2120–2130.
39. Ruiz-Uribe NE, Bracko O. Brain and blood extraction for immunostaining, protein, and RNA measurements after long-term two photon imaging in mice. *Protocol Exchange*. 2020. doi: 10.21203/rs.3.pex-838/v1.
40. Wang HL, Lai TW. Optimization of Evans blue quantitation in limited rat tissue samples. *Sci Rep*. 2014;4:6588.
41. Antonetti DA, Barber AJ, Hollinger LA, Wolpert EB, Gardner TW. Vascular endothelial growth factor induces rapid phosphorylation of tight junction proteins occludin and zonula occluden 1. A potential mechanism for vascular permeability in diabetic retinopathy and tumors. *J Biol Chem*. 1999;274(33):23463–23467.
42. Wolters FJ, Zonneveld HI, Hofman A, et al.; Heart–Brain Connection Collaborative Research Group. Cerebral perfusion and the risk of dementia: A population-based study. *Circulation*. 2017;136(8):719–728.
43. Korte N, Nortley R, Attwell D. Cerebral blood flow decrease as an early pathological mechanism in Alzheimer's disease. *Acta Neuropathol*. 2020;140(6):793–810.
44. Falkenhain K, Ruiz-Uribe NE, Haft-Javaherian M, et al.; Stall Catchers. A pilot study investigating the effects of voluntary exercise on capillary stalling and cerebral blood flow in the APP/PS1 mouse model of Alzheimer's disease. *PLoS One*. 2020;15(8): e0235691.
45. Bracko O, Njiru BN, Swallow M, Ali M, Haft-Javaherian M, Schaffer CB. Increasing cerebral blood flow improves cognition into late stages in Alzheimer's disease mice. *J Cereb Blood Flow Metab*. 2020;40(7):1441–1452.
46. Wittko-Schneider IM, Schneider FT, Plate KH. Brain homeostasis: VEGF receptor 1 and 2-two unequal brothers in mind. *Cell Mol Life Sci*. 2013;70(10):1705–1725.
47. Alvarez XA, Alvarez I, Aleixandre M, et al. Severity-related increase and cognitive correlates of serum VEGF levels in Alzheimer's disease ApoE4 carriers. *J Alzheimers Dis*. 2018;63(3): 1003–1013.
48. Cho SJ, Park MH, Han C, Yoon K, Koh YH. VEGFR2 alteration in Alzheimer's disease. *Sci Rep*. 2017;7(1):17713.
49. Moore AM, Mahoney E, Dumitrescu L, et al. APOE epsilon4-specific associations of VEGF gene family expression with cognitive aging and Alzheimer's disease. *Neurobiol Aging*. 2020;87:18–25.
50. Hohman TJ, Bell SP, Jefferson AL. Alzheimer's Disease Neuroimaging I. The role of vascular endothelial growth factor in neurodegeneration and cognitive decline: Exploring interactions with biomarkers of Alzheimer disease. *JAMA Neurol*. 2015; 72(5):520–529.
51. Chakraborty A, Chatterjee M, Twaalfhoven H, et al. Vascular Endothelial Growth Factor remains unchanged in cerebrospinal fluid of patients with Alzheimer's disease and vascular dementia. *Alzheimers Res Ther*. 2018;10(1):58.
52. Yang AC, Vest RT, Kern F, et al. A human brain vascular atlas reveals diverse cell mediators of Alzheimer's disease risk. *bioRxiv*. [Preprint] doi:10.1101/2021.04.26.441262
53. Burger S, Noack M, Kirazov LP, et al. Vascular endothelial growth factor (VEGF) affects processing of amyloid precursor protein and beta-amyloidogenesis in brain slice cultures derived from transgenic Tg2576 mouse brain. *Int J Dev Neurosci*. 2009;27(6):517–523.
54. Cifuentes D, Poittevin M, Dere E, et al. Hypertension accelerates the progression of Alzheimer-like pathology in a mouse model of the disease. *Hypertension*. 2015;65(1):218–224.
55. Chen MB, Yang AC, Yousef H, et al. Brain endothelial cells are exquisite sensors of age-related circulatory cues. *Cell Rep*. 2020; 30(13):4418–4432.e4.
56. Bennett RE, Robbins AB, Hu M, et al. Tau induces blood vessel abnormalities and angiogenesis-related gene expression in P301L transgenic mice and human Alzheimer's disease. *Proc Natl Acad Sci USA*. 2018;115(6):E1289–E1298.
57. Chiappelli M, Borroni B, Archetti S, et al. VEGF gene and phenotype relation with Alzheimer's disease and mild cognitive impairment. *Rejuvenation Res*. 2006;9(4):485–493.
58. Lau SF, Cao H, Fu AKY, Ip NY. Single-nucleus transcriptome analysis reveals dysregulation of angiogenic endothelial cells and neuroprotective glia in Alzheimer's disease. *Proc Natl Acad Sci USA*. 2020;117(41):25800–25809.
59. Mahoney ER, Dumitrescu L, Moore AM, et al. Brain expression of the vascular endothelial growth factor gene family in cognitive aging and Alzheimer's disease. *Mol Psychiatry*. 2019;26(3): 888–896.
60. Malamitsi-Puchner A, Tziotis J, Tsonou A, Protonotariou E, Sarandakou A, Creatsas G. Changes in serum levels of vascular endothelial growth factor in males and females throughout life. *J Soc Gynecol Investig*. 2000;7(5):309–312.
61. Bucci M, Roviezzo F, Posadas I, et al. Endothelial nitric oxide synthase activation is critical for vascular leakage during acute inflammation *in vivo*. *Proc Natl Acad Sci USA*. 2005;102(3):904–908.
62. Gonzalez-Mariscal L, Tapia R, Chamorro D. Crosstalk of tight junction components with signalling pathways. *Biochim Biophys Acta*. 2008;1778(3):729–756.
63. Elias BC, Suzuki T, Seth A, et al. Phosphorylation of Tyr-398 and Tyr-402 in occludin prevents its interaction with ZO-1 and destabilizes its assembly at the tight junctions. *J Biol Chem*. 2009; 284(3):1559–1569.
64. Nikolakopoulou AM, Wang Y, Ma Q, et al. Endothelial LRP1 protects against neurodegeneration by blocking cyclophilin A. *J Exp Med*. 2021;218(4):e20202207.
65. Raleigh DR, Boe DM, Yu D, et al. Occludin S408 phosphorylation regulates tight junction protein interactions and barrier function. *J Cell Biol*. 2011;193(3):565–582.

66. Beauchesne E, Desjardins P, Hazell AS, Butterworth RF. eNOS gene deletion restores blood–brain barrier integrity and attenuates neurodegeneration in the thiamine-deficient mouse brain. *J Neurochem*. 2009;111(2):452–459.
67. Takechi R, Galloway S, Pallebage-Gamarallage MM, et al. Differential effects of dietary fatty acids on the cerebral distribution of plasma-derived apo B lipoproteins with amyloid-beta. *Br J Nutr*. 2010;103(5):652–662.
68. Yamazaki Y, Shinohara M, Shinohara M, et al. Selective loss of cortical endothelial tight junction proteins during Alzheimer's disease progression. *Brain*. 2019;142(4):1077–1092.
69. Desai BS, Monahan AJ, Carvey PM, Hendey B. Blood–brain barrier pathology in Alzheimer's and Parkinson's disease: Implications for drug therapy. *Cell Transplant*. 2007;16(3):285–299.
70. Ni Y, Teng T, Li R, Simonyi A, Sun GY, Lee JC. TNFα alters occludin and cerebral endothelial permeability: Role of p38MAPK. *PLoS One*. 2017;12(2):e0170346.
71. Liu X, Dreffs A, Díaz-Coránguez M, et al. Occludin S490 phosphorylation regulates vascular endothelial growth factor-induced retinal neovascularization. *Am J Pathol*. 2016;186(9):2486–2499.
72. Nakao S, Arima M, Ishikawa K, et al. Intravitreal anti-VEGF therapy blocks inflammatory cell infiltration and re-entry into the circulation in retinal angiogenesis. *Invest Ophthalmol Vis Sci*. 2012;53(7):4323–4328.
73. Murakami T, Frey T, Lin C, Antonetti DA. Protein kinase cβ phosphorylates occludin regulating tight junction trafficking in vascular endothelial growth factor-induced permeability *in vivo*. *Diabetes*. 2012;61(6):1573–1583.
74. Jiang Y, Liu L, Steinle JJ. Compound 49b regulates ZO-1 and occludin levels in human retinal endothelial cells and in mouse retinal vasculature. *Invest Ophthalmol Vis Sci*. 2017;58(1):185–189.
75. Miyamoto K, Khosrof S, Bursell SE, et al. Prevention of leukostasis and vascular leakage in streptozotocin-induced diabetic retinopathy via intercellular adhesion molecule-1 inhibition. *Proc Natl Acad Sci USA*. 1999;96(19):10836–10841.
76. Lu M, Perez VL, Ma N, et al. VEGF increases retinal vascular ICAM-1 expression *in vivo*. *Invest Ophthalmol Vis Sci*. *Jul*. 1999;40(8):1808–1812.
77. Klohs J. An integrated view on vascular dysfunction in Alzheimer's disease. *Neurodegener Dis*. 2020;19(3-4):109–119.
78. Pietronigro E, Zenaro E, Bianca VD, et al. Blockade of α4 integrins reduces leukocyte–endothelial interactions in cerebral vessels and improves memory in a mouse model of Alzheimer's disease. *Sci Rep*. 2019;9(1):12055.
79. Zenaro E, Piacentino G, Constantin G. The blood–brain barrier in Alzheimer's disease. *Neurobiol Dis*. 2017;107:41–56.
80. Zenaro E, Pietronigro E, Della Bianca V, et al. Neutrophils promote Alzheimer's disease-like pathology and cognitive decline via LFA-1 integrin. *Nat Med*. 2015;21(8):880–886.
81. Chapouly C, Tadesse Argaw A, Horng S, et al. Astrocytic TYMP and VEGFA drive blood–brain barrier opening in inflammatory central nervous system lesions. *Brain*. 2015;138(Pt 6):1548–1567.
82. Rosenstein JM, Krum JM, Ruhrberg C. VEGF in the nervous system. *Organogenesis*. 2010 Apr–Jun 2010;6(2):107–114.
83. Koch S, Claesson-Welsh L. Signal transduction by vascular endothelial growth factor receptors. *Cold Spring Harb Perspect Med*. 2012;2(7):a006502.
84. Religa P, Cao R, Religa D, et al. VEGF significantly restores impaired memory behavior in Alzheimer's mice by improvement of vascular survival. *Sci Rep*. 2013;3:2053.
85. Garcia KO, Ornellas FL, Martin PK, et al. Therapeutic effects of the transplantation of VEGF overexpressing bone marrow mesenchymal stem cells in the hippocampus of murine model of Alzheimer's disease. *Front Aging Neurosci*. 2014;6:30.
86. Wang P, Xie ZH, Guo YJ, et al. VEGF-induced angiogenesis ameliorates the memory impairment in APP transgenic mouse model of Alzheimer's disease. *Biochem Biophys Res Commun*. 2011;411(3):620–626.
87. Jefferies WA, Price KA, Biron KE, Fenninger F, Pfeifer CG, Dickstein DL. Adjusting the compass: New insights into the role of angiogenesis in Alzheimer's disease. *Alzheimers Res Ther*. 2013;5(6):64.
88. St-Amour I, Paré I, Alata W, et al. Brain bioavailability of human intravenous immunoglobulin and its transport through the murine blood–brain barrier. *J Cereb Blood Flow Metab*. 2013;33(12):1983–1992.